



An Efficient Heterogeneous Cu-Grafted Mesoporous Organosilicas Nanocatalyst for Two and Three Component C—S Coupling Reactions

John Mondal¹, Noor Salam², and Asim Bhaumik^{1,*}

¹Department of Materials Science, Indian Association for the Cultivation of Science, Jadavpur 700032, India

²Department of Chemistry, University of Kalyani, Kalyani, Nadia 741235, W.B., India

Furfural-imine functionalized mesoporous organosilica material has been synthesized by post-synthesis surface functionalization of 2D-hexagonal mesoporous SBA-15 with organosilane precursor 3-aminopropyltriethoxy-silane (APTES) followed by Schiff-base condensation with furfural. On the other hand, furfural-imine functionalized MCM-41 has been synthesized by Schiff-base condensation of furfural and 3-aminopropyltriethoxy-silane (APTES) followed by its hydrothermal co-condensation with tetraethylorthosilicate (TEOS) in the presence of a cationic surfactant CTAB. Subsequent reaction of the imine-functionalized mesoporous organosilicas with Cu(OAc)₂ in absolute ethanol produced Cu(II)-grafted mesoporous nanocatalysts **1** and **2**, respectively. Powder XRD, HR TEM, FE SEM, N₂ sorption and EPR experimental tools are employed to characterize these Cu-grafted furfural-imine functionalized nanocatalysts. Cu-grafted MCM-41 (**1**) showed very good catalytic efficiency for the coupling of aryl bromides and thiophenol under aerobic conditions to produce different thioethers. On the other hand, Cu-anchored mesoporous SBA-15 nanocatalyst (**2**) exhibited high catalytic activity for one-pot three component coupling of different aryl halides with thiourea and benzyl bromide in aqueous medium to produce different aryl alkyl thioethers in very good yields. Both Cu-grafted mesoporous nanocatalysts can be efficiently reused for several reaction cycles.

Keywords: Aryl Alkyl Thioethers, Cu-Grafting, C—S Bond Formation, 2 and 3 Component Coupling Reactions, Furfural Imine Functionalized Mesoporous Organosilica.

1. INTRODUCTION

Over a decade of extensive research nanomaterials have emerged as one of the most useful and promising materials because of their unique surface properties, which are widely different from their corresponding bulk systems.^{1,2} Due to their versatile potentials, nanomaterials are employed extensively in numerous frontline areas such as electronic, optical, catalytic, coating, medical, sensor applications, etc.³ High surface-to-volume ratio and unique 1-, 2- or 3-dimensional morphological features make the metal grafted nanoparticles more attractive catalysts compared to the catalysts based on the respective bulk materials.^{4,5} Further, different types of organic and inorganic reactions catalyzed by self-assembled nanoparticles are gaining increasing importance in recent times.⁶ Currently Cu/CuO nanoparticles have attracted a considerable awareness in the field of catalysis^{7,8} and as

well as in the energy conversions.⁹ From the past one decade it is believed that copper, in the nanoform provides fascinating catalytic activity in various organic transformations. Due to the low cost of copper compared to Au, Ag, Pd, Pt, Ru and Rh, Cu-containing compounds/materials has attracted particular attention as catalyst for various organic reactions.^{10,11} The size and shape of these nanocatalysts became an important aspect in catalyst design, which provides a highly active catalyst surface, increasing the reaction rates and decreasing the consumption of the catalyst.^{12,13} Furthermore, Cu-grafted functionalized heterogeneous catalysts provide the advantages of simplified isolation of the product, easy recovery, enhanced stability and recyclability of the catalysts over their respective homogeneous counterpart. Thus, researchers are keener for the development of heterogeneous catalysts with the long catalyst life and reusability for several cycles minimizing E factor.^{14,15} Many organic transformations can be performed by employing heterogeneous copper catalysts such as supported CuNPs,¹⁶

*Author to whom correspondence should be addressed.

nanostructured CuO materials,¹⁷ Cu/C,¹⁸ Cu/CuO,¹⁹ hetero bimetallic Cu–Ni/C²⁰ and Cu/AlO(OH).²¹ One major drawback in the heterogenization of Cu at the surface of functionalized nanomaterials is that the nanoparticles have the tendency to leach out irreversibly from its heterogeneous support, preventing long-lived recyclable use of the nanocatalyst. This feature is sensitive to the ligand environment of the copper ions, which strongly affect the dispersion of the copper species in the solid surface. So many important factors such as the chemical nature of the support to entrap the copper nanoparticles, its acid-base functionality (i.e., donor sites such as O, N, S atoms etc.) as well as the location of copper nanoparticles into the channel of porous system play crucial role in catalyst life and stability of the Cu-grafted nanocatalysts.²³

In the last two decades considerable research work have been devoted to synthesize mesoporous materials with tunable pore size distribution that can be used as a suitable host matrix for anchoring metal/metal oxide species due to their exceptionally high surface area, higher hydrothermal and mechanical stability.^{24,25} Among them, SBA-15 type silicas with the large mesopore can be synthesized using poly (alkylene oxide) triblock copolymers as a structure directing agent.^{26–28} The size, shape and connectivity of the existing pores into the mesoporous materials can be tuned through some chemical reactions in such a way that can stabilize metal/metal oxide nanoparticles via anchoring of the functional groups on the external surface and as well as into the pores. The properties of these mesoporous silica supported nanocomposites can be controlled not only by using the desired active ligands, which can encapsulate the nanoparticles strongly but also dispersion of uniform metal/metal oxide nanoparticles with the preservation of the porous host structure. In recent times, two different synthetic strategies are employed for the preparation of Cu-grafted functionalized mesoporous silicas. Well dispersed CuO nanoparticles can be efficiently prepared by “direct synthetic” method, which is industrially more practicable as it is relatively easy and convenient to handle. CuO loaded mesoporous silicas like MCM-41 and MCM-48 have been designed by using this strategy.^{29–31} Synthesis of Cu-rich functionalized mesoporous material without the distortion of the pore ordering of the support becomes a tedious job as copper salts have the tendency to leach out in acidic medium. Today considerable efforts have been devoted for the synthesis of Cu(II)-rich SBA-15 and KIT-6 materials by tuning “direct synthetic” method.³² Post synthetic strategies are also applied for the synthesis of highly dispersed Cu nanoparticles supported over ordered mesoporous materials as host.³³ Very recently, some attempts have been made to design mesoporous composite nanomaterials through the grafting of metal ions on preliminary functionalized silica surface.³⁴ Mesoporous silica has been functionalized in such a way that the active metal ion can bind tightly with silica inside the cavity present at the mesopore surface so that it cannot

be leached out from the mesopores during the reaction conditions.

In this context it is pertinent to mention that C–S bond formation reaction becomes an indispensable tool in organic synthesis today and its importance is felt in designing diverse array of target molecules ranging from biological to pharmaceutical interestes³⁵ as well as for the development of new molecular precursor in the materials science.^{36,37} A large variety of aryl sulfides can be employed as drugs for the treatment of diabetes, inflammation, Alzheimer’s and Parkinson’s disease,³⁸ cancer³⁹ and HIV disease.³⁴ In this context, transition metal catalyzed C–S cross coupling^{40–43} reactions have been studied to a less extent compared to C–C, C–N and C–O cross coupling reactions. Favorable S–S oxidative coupling reaction resulting in the undesired formation of disulfides and simultaneous deactivation of metal catalyst as organic sulfur compounds are effective metal binders, make the C–S cross coupling reaction quite inauspicious. C–S cross-coupling has been performed with the use of several transition metal catalysts such as palladium,^{44,45} nickel,⁴⁶ copper,⁴¹ cobalt,⁴² iron,⁴⁷ and indium⁴⁸ etc. The catalytic system associated with the palladium catalysts for performing C–S cross coupling reaction has been employed to a limited extent due to the high cost, air sensitivity of palladium salts and the use of environmentally harmful organophosphorous ligands. Further, turnover numbers (TON) for the Ni and Co catalysts in these reactions are low. Due to the low cost and easy availability of copper salts it has the potential to be used for the large scale catalytic process but the problems associated with these catalysts are high reaction temperature, long reaction time and severe reaction conditions. So the copper containing heterogeneous catalyst must be designed in such a way that will be inexpensive, non-air sensitive and recyclable. C–S cross coupling reaction can be performed through the catalytic reaction of aryl halides with thiophenol in the presence of a base. But the direct use of volatile and foul-smelling thiols, which hinders environmental and safety problems and limits the use of this method for large scale operation. In this context two interesting protocols have been developed for the C–S bond formation reactions catalyzed by Cu-grafted nanocatalysts. One is the one-pot Michael addition reaction via an odourless process involving *in situ* generation of S-alkylisothiuronium salts in water⁴⁹ and another one is one-pot thioetherification of aryl halides using thiourea (free from the foul smell of thiols).⁵⁰ In these processes thiourea has been used instead of thiol and thiourea undergoes reaction with the aryl halides to generate thiol moiety *in situ* and makes the catalytic process free from foul smell. Thus, designing an efficient and environmentally friendly Cu nanocatalyst for C–S cross coupling reaction without using foul smell thiol is highly desirable to address these environmental and industrial concerns.

Herein, we report the synthesis and detailed characterizations of two Cu-grafted mesoporous nanocatalyst employing both “*in-situ* grafting” and “post grafting” methods. Furfural-imine functionalized mesoporous material has been synthesized by Schiff-base condensation of furfural and 3-aminopropyltriethoxy-silane (APTES) followed by its hydrothermal co-condensation with tetraethylorthosilicate (TEOS) in the presence of a cationic surfactant CTAB. This mesoporous nanoparticles was functionalized by reaction with $\text{Cu}(\text{OAc})_2$ to obtain Cu-grafted MCM-41 (**1**), which acts as efficient catalyst for the C–S cross coupling sulfides. In another case “post grafting” method has been applied to synthesize Cu-grafted SBA-15 nanocatalyst (**2**). This heterogeneous catalyst was developed by surface functionalization with 3-aminopropyl-triethoxysilane (APTES) followed by Schiff-base condensation with furfural. This functionalized SBA-15 material was treated with $\text{Cu}(\text{OAc})_2$ to provide Cu-grafted SBA-15 nanocatalyst (**2**), which catalyzes one-pot three component thioetherification reaction of aryl halides with benzyl bromide and thiourea in aqueous medium in the presence of K_2CO_3 base.

2. EXPERIMENTAL DETAILS

2.1. Synthesis of Cu-Grafted Mesoporous MCM-41 Nanocatalyst (**1**)

2.1.1. Synthesis of Schiff Base Ligand (**A**)

A solution of APTES (0.01 mol, 2.21 g, Aldrich) in dry ethanol (5 ml) was added dropwise into the furfural solution (0.01 mol, 0.9609 g taken in dry ethanol 20 ml) over 20 min under vigorous stirring condition. After the complete addition of organic ligand the reaction mixture was refluxed for about 8 h. Then reaction mixture was allowed to cool at room temp and excess solvent was evaporated to dryness, leaving behind a dark brown colored viscous gel. This dark brown colored viscous liquid was designated as (**A**) and it was characterized by ^1H and ^{13}C NMR.

2.1.2. Synthesis of Furfural Functionalized Mesoporous Organic Hybrid Silica (**B**)

In a typical synthesis procedure structure directing agent CTAB (Loba Chemie, 0.0075 mol, 2.73 g) was added in an aqueous solution of tartaric acid (0.6 g in 20 g H_2O) and the resulting mixture was allowed to stir for about 30 min. After the solution becomes clear, dark brown color viscous gel (**A**) (1.35 g) in 5 mL ethanol was added dropwise into the surfactant solution and the resulting mixture was stirred for about 2 h. Then 5.245 g TEOS (0.025 mol) was added in the previous solution and it was stirred for about 2 h to obtain a brown colored viscous gel. After that TMAOH solution was added dropwise into the gel to make the pH

of the gel at 12.0. The resulting gel was left under stirring for another 12 h at room temperature and then it was autoclaved at 353 K for 72 h under static condition. After 72 h it was cooled at room temperature and filtered to offer yellow colored solid. The template CTAB was removed from as-synthesized sample by extracting the solid mass for three times with ethanolic solution of HCl at room temperature and this sample has been designated as (**B**).

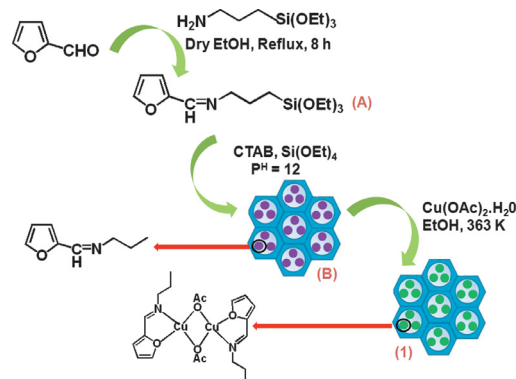
2.1.3. Synthesis of Cu-Grafted Mesoporous MCM-41 Nanocatalyst (**1**)

Furfural-imine functionalized mesoporous silica **B** (1 g) was dispersed in ethanol (20 ml) solution through continuous stirring at room temperature for 30 min. Then copper (II) acetate (0.2 g) was added into the mixture and the stirring was continued at the room temperature to obtain a homogeneous blue colored solution. It was refluxed for about 8 h at 363 K. The color of the mesoporous material was slowly changed from yellow to light green and no further color change occurred on further reflux. The reaction mixture was cooled at room temperature and the resulting light green colored mesoporous solid was isolated through filtration under suction. After washing several times with ethanol it was dried under vacuum. The light green colored mesoporous material was designated as Cu-grafted mesoporous MCM-41 nanocatalyst **1**. The outline for the preparation of this furfural-imine functionalized Cu nanocatalyst is shown in Scheme 1.

2.2. Synthesis of Cu-Grafted Mesoporous SBA-15 Nanocatalyst (**2**)

2.2.1. Synthesis of 3-Aminopropyl Functionalized SBA-15

Calcined mesoporous silica SBA-15 was synthesized by the reported procedure as described before.²⁷ 0.18 g of 3-aminopropyltriethoxysilane (3-APTES) was added into the calcined SBA-15 (0.1 g) dispersed into CHCl_3 (10 mL)



Scheme 1. Synthesis of Cu-F-MCM-41 nanocatalyst (**1**).

and the mixture was stirred at room temperature under N_2 atmosphere for about 12 h. The resulting white solid was isolated by filtration from the reaction mixture, washed with chloroform followed by dichloromethane and finally dried in air. The white colored solid was designated as **I**.

2.2.2. Synthesis of Furfural-Imine Functionalized Mesoporous SBA-15 (**D**)

A solution of furfural (0.00081 mol, 0.077 g) taken in methanol (5 ml) was added dropwise into the 3-APTES functionalized SBA-15 material **I** dispersed into methanol (15 ml) under vigorous stirring condition at room temperature. After the complete addition of furfural the reaction mixture was refluxed for about 6 h at 333 K. After 10–15 minutes the color of the reaction mixture was changed into deep yellow and no further color change occurred on further reflux after 6 h. The reaction mixture was cooled at room temperature and the final yellow product was filtered by repeatedly washing with hot methanol to remove the unreacted aldehyde. The yellow colored material was dried in air and was designated as (**D**).

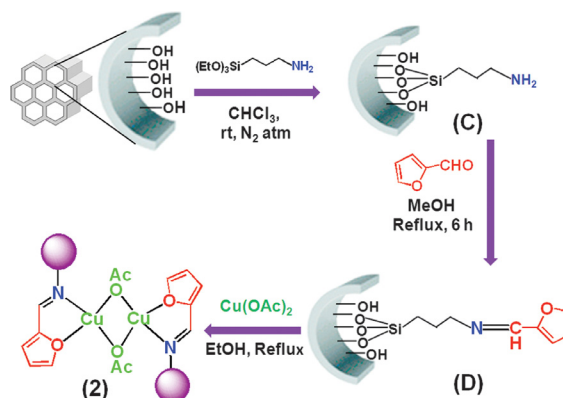
2.2.3. Synthesis of Cu-Grafted Mesoporous SBA-15 Nanocatalyst (**2**)

Dried furfural-imine functionalized mesoporous SBA-15 (**D**) (1 g) was dispersed in the absolute ethanol (20 ml). Then 0.2 g of copper (II) acetate was added into the previous reaction mixture. Then the resulting reaction mixture was kept under refluxing condition for about 8 h at 363 K. The color of the mesoporous material was slowly changed from deep yellow to light green and no further color change occurred on further reflux. The reaction mixture was cooled at room temperature and the resulting mesoporous material was filtered through suction and thoroughly washed with ethanol. After washing it was dried at the room temperature. The light green colored mesoporous material has been designated as Cu-grafted mesoporous SBA-15 nanocatalyst (**2**). The outline for the preparation of this Cu-grafted SBA-15 nanocatalyst is shown in Scheme 2.

2.3. Catalytic Testing Procedure

2.3.1. Two Component C—S Coupling Reaction of Aryl Bromides with Thiophenol

A solution of bromobenzene (204 mg, 1 mmol), thiophenol (121 mg, 1.1 mmol) and K_2CO_3 (276 mg, 2 mmol) in 3 ml DMF was stirred at room temperature for 1 h. Then Cu-grafted MCM-41 nanocatalyst **1** (20 mg) was added into the reaction mixture and it was heated at 383 K in an oil bath under aerobic condition. The progress of the reaction was monitored by TLC. After a period of time the reaction mixture was allowed to cool, quenched



Scheme 2. Synthesis of Cu-F-SBA-15 nanocatalyst (**2**).

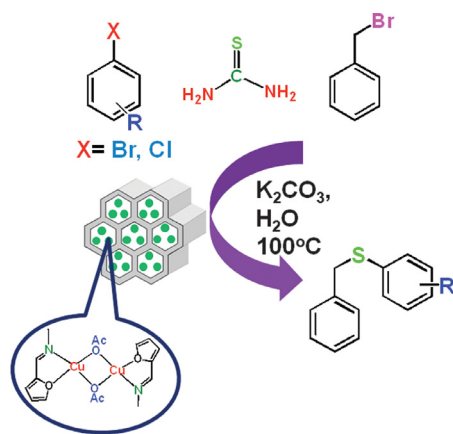
with the addition of 2 ml water and catalyst was separated by simple filtration. The filtrate was diluted with EtOAc (20 ml) and it was extracted with EtOAc with the addition of 10% aqueous NaOH solution for several times to remove the solvent DMF. The combined organic layer was washed with water and brine solution. Then the combined organic layer was dried over anhydrous Na_2SO_4 and evaporated to dryness to offer the crude product diphenyl sulfide as colorless oil. The isolated crude product was characterized by 1H and ^{13}C NMR respectively. The C—S coupling reaction between thiophenol with aryl bromides over catalyst **1** is shown in the Scheme 3.

2.3.2. One-Pot Three Component Thioetherification in Aqueous Medium

At first K_2CO_3 (552 mg, 4 mmol) and thiourea (91 mg, 1.2 mmol) were dissolved in 5 ml water. Then aryl halide (1 mmol), benzyl bromide (188 mg, 1.1 mmol) and Cu-grafted SBA-15 nanocatalyst (**2**) (25 mg) were added into the previous aqueous solution and the resulting mixture was heated at 373 K in an oil bath for the desired reaction time. Progress of the reaction was monitored using TLC. After completion of the reaction, the reaction mixture was cooled to room temperature and it was extracted with EtOAc. The combined organic layer was washed with water to remove excess unreacted thiourea and then followed by brine solution. Then the combined organic layer was dried over anhydrous Na_2SO_4 and evaporated to dryness to offer the preferred aryl alkyl thioethers as colorless oil. The isolated crude product was characterized by 1H and ^{13}C NMR respectively. The reaction pathway for the



Scheme 3. C—S coupling reaction of bromobenzene with thiophenol over Cu-F-MCM-41 nanocatalyst (**1**).



Scheme 4. One pot thioetherification reaction of aryl halides using thiourea and benzyl bromide over Cu-F-SBA-15 nanocatalyst (**2**) in aqueous medium.

one-pot thioetherification reaction of aryl halide by using thiourea and benzyl bromide over catalyst (**2**) in aqueous medium is shown in the Scheme 4.

2.4. Characterization Techniques

Powder X-ray diffraction patterns are recorded on a Bruker D-8 Advance SWAX diffractometer operated at 40 kV voltages and 40 mA current. The instrument has been calibrated with a standard silicon sample, using Ni-filtered Cu K_{α} ($\lambda = 0.15406$ nm) radiation. Nitrogen adsorption/desorption isotherms were obtained using a Quantachrome Autosorb 1 C at 77 K. Prior to gas adsorption, all the samples were degassed for 10 h at 423 K. A JEOL JEM 6700F field emission scanning electron microscope is used for the determination of morphology of the particles. High resolution transmittance electron microscopic (HR TEM) images were recorded in a Jeol JEM 2010 transmission electron microscope. Cu loading in the sample was estimated by using a Perkin-Elmer Optima 2100 DV Inductive Coupled Plasma Atomic Emission Spectroscopy (ICP-AES). ^1H and ^{13}C NMR experiments were carried out on a Bruker DPX-300 NMR spectrometer. EPR measurements were performed on a Bruker EMX EPR spectrometer at X-band frequency (9.46 GHz) at liquid nitrogen temperature (77 K).

3. RESULTS AND DISCUSSION

3.1. Characterisation of Catalysts

The small-angle powder X-ray diffraction (SAXRD) pattern of Cu-grafted SBA-15 nanocatalyst (**2**) showed a single intense peak ($2\theta = 0.9$) corresponding 100 (strong) plane (Fig. 1(a)). This result suggests that the mesophase has been preserved on grafting of Cu at the functionalized SBA-15 surface. But the intensities of the other peaks

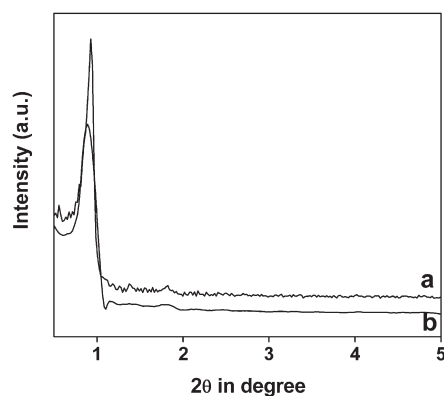


Fig. 1. Small angle powder XRD pattern of Cu-F-SBA-15 nanocatalyst (a) and reused nanocatalyst after catalytic reaction (b).

corresponding to 110 and 200 planes have been decreased from that before Cu-loading. This considerable decrease in the peak intensities on grafting of Cu at the surface could be attributed to the lowering of local order. The PXRD pattern of this material after six repetitive reaction cycles is shown in Figure 1(b). From this pattern it is clear that the Cu-nanocatalyst retains its mesoporous structure after repeated recycles. The wide angle XRD pattern of the Cu grafted SBA-15 nanocatalyst suggests that new orthorhombic phase has been generated on the pore wall (Fig. 2(a)). This nanocatalyst retains its nanostructures and crystalline phase after catalytic recycling (Fig. 2(b)).

N_2 adsorption/desorption isotherms of the Cu-grafted SBA-15 nanocatalyst and its reused form are shown in the Figure 3. Both these samples showed typical type IV isotherms with very large hysteresis loops in the 0.5 to 0.8 P/P_0 range. The isotherms account for the relatively ordered mesopore and the hysteresis loop is the characteristic for the large tubular pores of SBA-15. The BET surface areas for the Cu-grafted SBA-15 nanocatalyst and

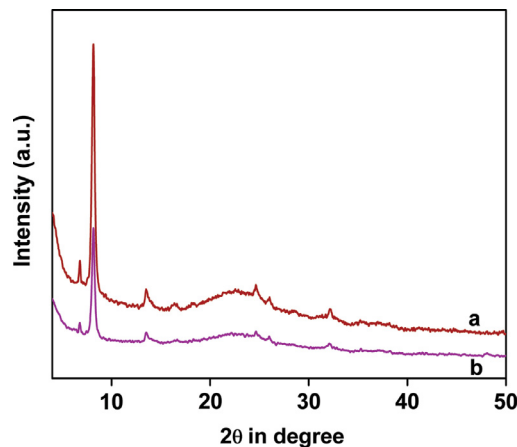


Fig. 2. Wide angle powder XRD patterns of Cu-F-SBA-15 nanocatalysts: fresh (a) and reused (b).

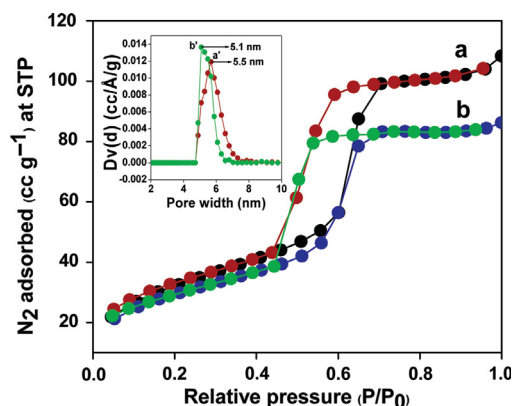


Fig. 3. N_2 adsorption/desorption isotherms of Cu-F-SBA-15 nanocatalyst: fresh (a) and reused (b). Pore size distributions estimated through NLDFT method is shown in the inset.

reused catalyst (Figs. 3(a) and (b)) are $118 \text{ m}^2 \text{ g}^{-1}$ and $107 \text{ m}^2 \text{ g}^{-1}$, respectively and their corresponding pore size dimensions (calculated by the NLDFT method and shown in the inset of the Fig. 3) are 5.5 nm and 5.1 nm, respectively. A small decrease in the BET surface area

observed here clearly suggests that there is no change in the surface nanostructure and mesophase of the Cu-F-SBA-15 material during the course of reaction.⁵¹

TEM images of the Cu-F-SBA-15 nanocatalyst are shown in the Figure 4. Figure 4(A) clearly advocates that the honeycomb-like hexagonally ordered mesopores having dimensions 4.0–4.6 nm are arranged in the respective Cu nanocatalyst.⁵² The FFT diffractogram (inset of Fig. 4(A)) predicts that the 2D-hexagonal pore channels are present in the Cu-F-SBA-15 nanocatalyst. The black colored spots present in the Figures 4(A) and (B) are due to the chelation of furfural-grafted imine ligand with Cu^{2+} ion and these black color Cu nanoclusters are uniformly distributed throughout the sample. Figure 4(C) clarifies that the material has rod shaped particle morphology, which is due to the chelation of the imine ligand with Cu^{+2} ion and as a result the growth of the nanocluster occurs in the 1D way leading to the growth of the 1D nanorod. The pore dimensions and distribution of the Cu nanoclusters remains same in the reused catalyst (Fig. 4(D)).⁵³

The EPR spectra of the Cu-F-SBA-15 nanocatalyst are shown in the Figure 5. EPR spectrum of Cu-F-SBA-15 nanocatalyst displayed four splitting patterns

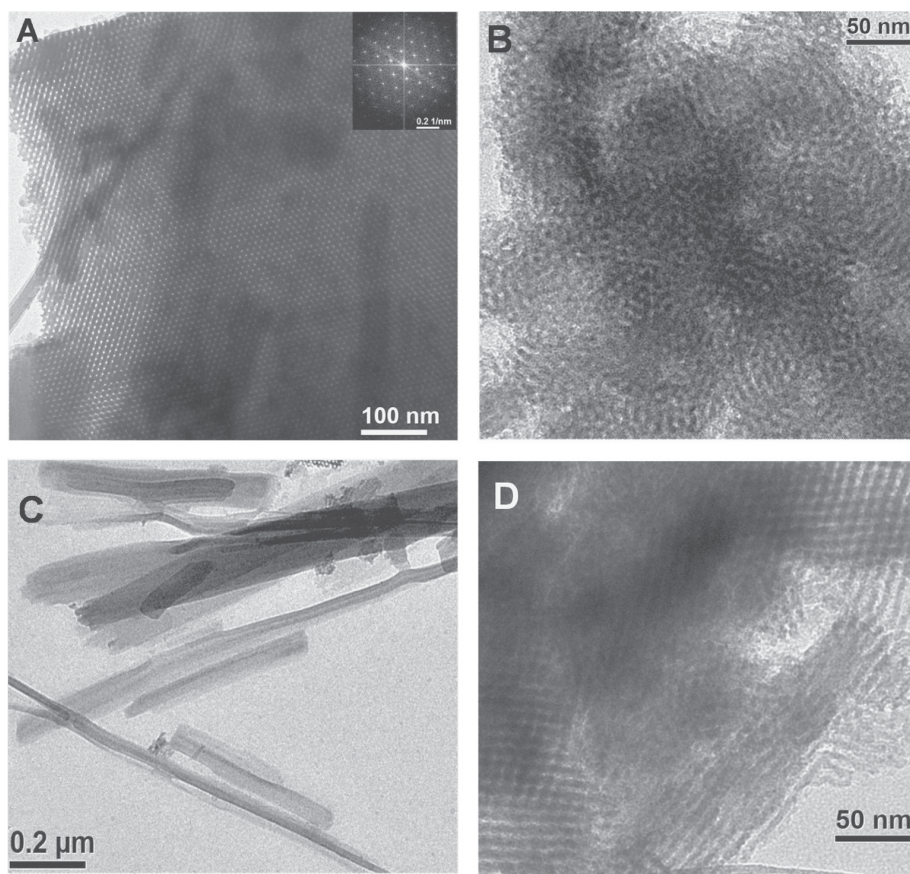


Fig. 4. HR TEM images of Cu-F-SBA-15 nanocatalyst (A), FFT pattern is shown in the inset), (B) and (C). TEM image of reused catalyst (D) after sixth catalytic cycles.

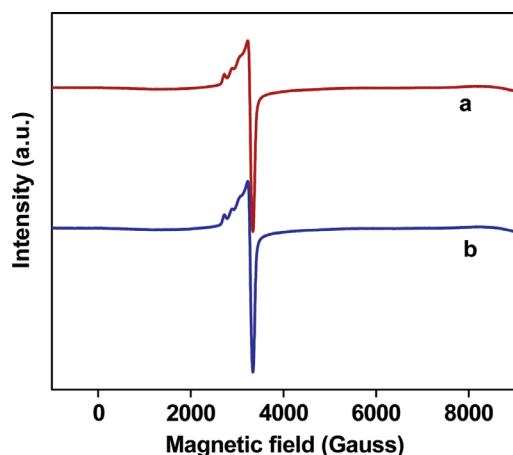


Fig. 5. EPR spectrum of Cu-F-SBA-15 nanocatalyst: fresh (a) and reused (b).

($mI = -3/2, -1/2, +1/2, +3/2$) in the low-field region (Fig. 5(a)) for the parallel component due to the hyperfine interaction between the unpaired electron and the nuclear spin of copper ($I = 3/2$). But the signals for the perpendicular component ($g_{\perp} = 2.06$) remain unresolved. These are the characteristics signals typical for isolated Cu^{2+} cations in the axial symmetry. EPR spectrum of Cu-F-SBA-15 nanocatalyst (Fig. 5(a)) showed: $g_{\parallel} = 2.26$ and $A_{\parallel} = 172$ G, which could provide us the information that the Cu(II) ions are arranged in the distorted square planar geometry. Therefore large pore of Cu-F-SBA-15 nanocatalyst (4.6 nm) offers a confinement effect to change a flexible geometry from square pyramidal to a more distorted pattern. In the EPR spectrum of the reused catalyst (Fig. 5(b)) the four splitting patterns and the g_{\perp} , g_{\parallel} and A_{\parallel} values remain unaltered, suggesting that there is no change in the geometry and the environment of the catalyst during the course of the reaction.⁵⁴

The FE SEM images of Cu-F-SBA-15 nanocatalyst and reused catalyst are shown in the Figure 6. The FE SEM image of the Cu-F-SBA-15 nanocatalyst (Fig. 6(A)) predicts us that this material has nanorod shape morphology. Due to the strong coordinating ability of furfural-imine functionalized SBA-15 it can form a complex with the Cu^{+2} ion. As a result spherical nanoparticles coordinate with the Cu^{+2} ion and leads to the growth of the nanoparticles in 1D direction, resulting in the formation of nanorods. We are quite aware about the fact that imine functionalized ligand molecules also behaved as the capping agents that can selectively adsorbed onto the lateral surfaces of the 1D Cu nanostructures causing complete inhibition of lateral growth of the nuclei. As a result this growth of the product continues along the c -axis in the direction of 001 plane.⁵⁵ Thus, our imine functionalized silica served not only as the coordinating agent but also as capping ligand, which played a crucial role for the 1D growth of the spherical nanoparticles for the formation of

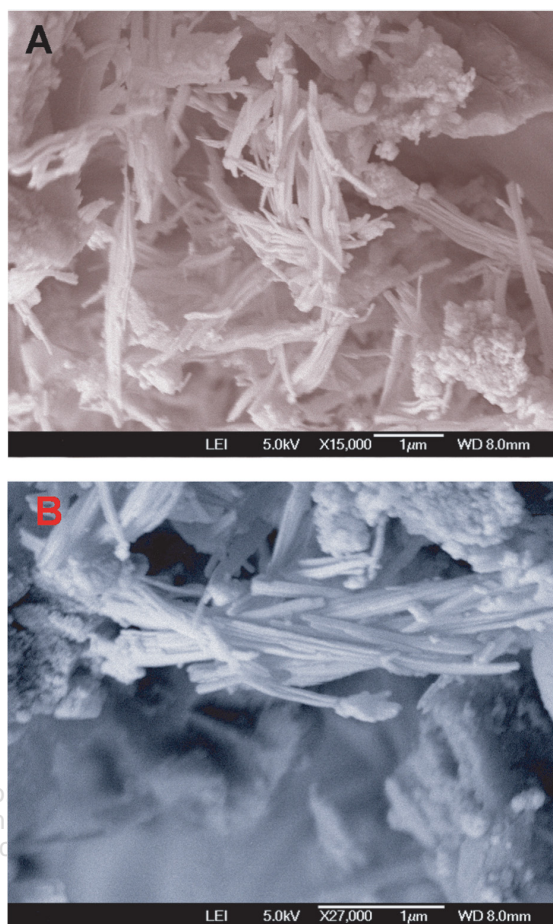


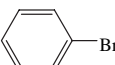
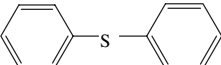
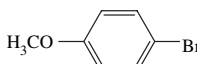
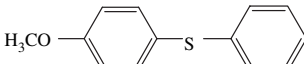
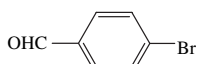
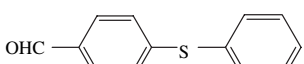
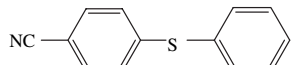
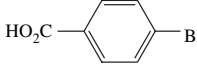
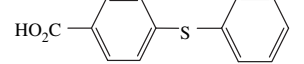
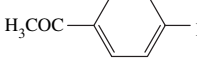
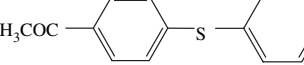
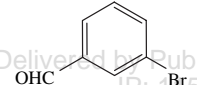
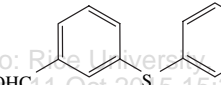
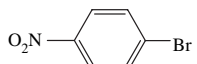
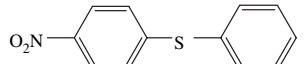
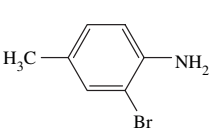
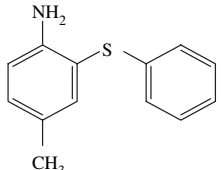
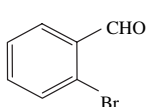
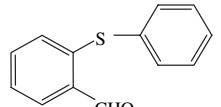
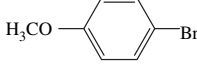
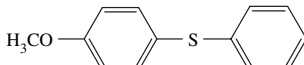
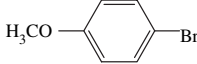
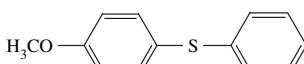
Fig. 6. FE SEM images of Cu-F-SBA-15 nanocatalyst (A) and reused Cu-F-SBA-15 nanocatalyst (B).

large nanorods. The FE SEM image (Fig. 6(B)) of the reused Cu-F-SBA-15 nanocatalyst suggests that the rod shape morphology has been preserved after the catalysis.⁵⁶

3.2. Catalytic Evaluations

C—S coupling reaction of different aryl bromides with thiophenol in DMF (Scheme 3) was explored over the Cu-F-MCM-41 nanocatalyst (**1**) to produce different substituted aryl thioether in excellent yields for various electron donating and electron withdrawing compounds (Table I). All these products are characterized by ^1H and ^{13}C NMR spectroscopy.⁵⁷ The C—S coupling reaction was completed within 8–10 h for all the aryl bromides and the turn over frequencies are moderately high (Table I). It was found that 0.02 g is the optimum amount of Cu-F-MCM-41 nanocatalyst required to perform this C—S coupling reaction. The increase of catalyst amount does not improve the yield of the products any further, whereas decreasing the amount of catalyst leads to decrease in the product yield. Under optimized reaction conditions for

Table I. C—S coupling reaction of aryl bromides with thiophenol over Cu-F-MCM-41 nanocatalyst under aerobic conditions.^a

Entry	Aryl bromides	Time (h)	Product	Yield ^b (%)	TON
1		8		82	37.9
2		8		88	40.7
3		10		86	39.8
4		8		85	39.3
5		9		85	39.3
6		10		84	38.8
7		8		82	37.9
8		11		78	36.1
9		10		75	34.7
10		8		82	37.9
11 ^d		8		58	26.8
12 ^e		16		20	9.2

Notes: ^aReaction conditions: aryl bromide (1 mmol, bromobenzene, 157 mg, entry 1), thiophenol (1.1 mmol, 121 mg), K₂CO₃ (2 mmol, 276 mg), DMF (3 ml), reaction temperature: 110 °C (oil bath), Cu-F-MCM-41 nanocatalyst (1): 20 mg; ^bIsolated yield of the product, ^cTurn over number (TON) = moles of substrate converted per mole of active site; ^dReaction conditions: 4-bromoanisole (1 mmol, 187 mg), thiophenol (1.1 mmol, 121 mg), K₂CO₃ (2 mmol, 276 mg), DMF (3 ml), reaction temperature: 333 K (oil bath), Cu-F-MCM-41 nanocatalyst: 20 mg; ^eReaction conditions: 4-bromoanisole (1 mmol, 187 mg), thiophenol (1.1 mmol, 121 mg), K₂CO₃ (2 mmol, 276 mg), DMF (3 ml), reaction temperature: 298 K (room temperature), Cu-F-MCM-41 nanocatalyst: 20 mg.

the C—S coupling reaction the time taken and the product yield obtained are listed in the Table I. The aldehydes with both electron donating (Table I, entries 2 and 9) and electron withdrawing groups (Table I, entries 3, 4, 5, 6, 7, 8 and 10) participated in the C—S coupling reaction with equal efficiency. Thus, the nature and position of substitution in the aromatic ring did not affect the reactions much. The *meta*-substituted aromatic aldehyde (Table I, entry 7) as well as sterically hindered *ortho*-substituted aromatic aldehydes (Table I, entries 9 and 10), both undergo arylthiolation very smoothly. *Ortho*-substituted bromo benzene bearing $-\text{NH}_2$ moiety in the aromatic ring was compatible in this coupling reaction without any reaction with the $-\text{NH}_2$ group (Table I, entry 9). The C—S coupling reaction can be performed with the several sensitive functional groups attached with the aromatic ring (Table I, entries 3, 4, 7, 8 and 10). The reaction was conducted by taking 4-bromoanisole and thiophenol in the presence of Cu-F-MCM-41 nanocatalyst at 333 K and 298 K temperature, providing yield 58% and 40% respectively (Table I, entries 11 and 12). From these above results we can conclude that the Cu-F-MCM-41 nanocatalyst is highly reactive at elevated temperature and 383 K is the optimum temperature required for the promotion of C—S coupling reaction. In order to understand the origin of catalytic activity in the Cu nanoclusters grafted into the functionalized MCM-41 silica, a control experiment for the C—S coupling reaction was performed by taking bromobenzene and thiophenol in absence of any catalyst in DMF solvent at 383 K (Table II, entry 1). Under this condition no reaction occurs and the starting components remain unreacted. We have also carried out the reaction in the presence of pure mesoporous silica MCM-41 (Table II, entry 2) and furfural-imine functionalized MCM-41 (Table II, entry 3) for bromobenzene and thiophenol in DMF at 383 K. However, no corresponding diphenyl sulfide was obtained under these conditions

too. This data clearly suggests that the Cu nanoclusters present at the catalyst surface play a crucial role to conduct this C—S coupling reaction. We have performed the C—S coupling reaction in DMF solvent for bromobenzene and thiophenol by using the homogeneous Cu-catalyst such as $\text{Cu}(\text{OAc})_2 \cdot \text{H}_2\text{O}$ (Table II, entry 4). But the homogeneous phase Cu catalyst $\text{Cu}(\text{OAc})_2 \cdot \text{H}_2\text{O}$ showed much lower catalytic activity than our Cu-F-MCM-41 nanocatalyst. When $\text{Cu}(\text{OAc})_2 \cdot \text{H}_2\text{O}$ was used as a catalyst in the C—S coupling reaction of iodobenzene and thiophenol then only 35% yield of the product was obtained (Table II, entry 5). Similarly, when $\text{Cu}(\text{OAc})_2 \cdot \text{H}_2\text{O}$ is used as catalyst at room temperature (298 K) in DMF no product was observed (Table II, entry 6). When Cu nanoparticle was anchored with the simple MCM-41 silica through simple impregnation, resulting catalyst showed only 45% product yield of the coupling product (Table II, entry 7). This experimental data predicts us that furfural-imine functionalized Cu nanocatalyst showed best results in terms of product yield and reaction rate compared to simple MCM-41 anchored Cu nanoparticles for this two component C—S coupling reaction.⁵⁸ So functionalization with the organic ligand is more important to anchor Cu nanoparticles strongly with a uniform distribution at the mouth of the mesopores for the promotion of two component C—S coupling reaction. With this sequence various bis-thioethers were achieved as illustrated in Scheme 3. This coupling reaction provides enormous scope for an easy access to a library of bithioethers and will have much potential in organic synthesis such as for the synthesis of poly-(*p*-phenylene sulfide) polymers. ICP-AES analysis revealed that the Cu content of this catalyst was 1.08 mmol g^{-1} . The TONs for various unsymmetrical diarylsulfides over catalyst **1** are listed in the Table I (varies between 37.9–9.2).

One-pot thioetherification (Scheme 4) of different aryl halides (chloro and bromo substituted arenes) using benzyl bromide in the presence of thiourea in aqueous medium at 100°C over Cu-F-SBA-15 nanocatalyst (**2**) gave different aryl alkyl substituted thioethers in good yields. The reaction condition for this one-pot thioetherification reaction was optimized with the reaction of benzyl bromide (1.1 mmol, 188 mg), thiourea (1.2 mmol, 91 mg), bromobenzene (1 mmol, 157 mg) in the presence of K_2CO_3 base (4 mmol, 552 mg) over Cu-F-SBA-15 nanocatalyst (25 mg) in H_2O under aerobic condition. The reaction proceeded smoothly and gave phenyl benzyl thioether with 82% yield.⁵⁹ We have studied the exposure of the reaction by applying various functional group substituted bromo- and chloro-arenes. Electron withdrawing functional groups such as $-\text{NO}_2$, $-\text{CHO}$, $-\text{COCH}_3$, $-\text{CN}$ attached with the bromo- and chloro-arenes participated in the C—S coupling reaction very smoothly. Electron donating substituents such as $-\text{OCH}_3$, $-\text{CH}_3$, $-\text{OH}$, $-\text{NH}_2$ on the aromatic ring were compatible for this reaction and gave uniformly high yield under this reaction condition. Heterocyclic bromo compound (bromo pyrazole) underwent this

Table II. Screening of different catalyst sources for the C—S coupling reaction of aryl bromide with thiophenol over Cu-F-MCM-41 nanocatalyst.^a

Entry	Catalyst	Time (h)	Yield (%)
1	No catalyst	15	0.0
2	MCM-41	15	0.0
3	Furfural-MCM-41	15	0.0
4	$\text{Cu}(\text{OAc})_2 \cdot \text{H}_2\text{O}$	15	25.0
5	$\text{Cu}(\text{OAc})_2 \cdot \text{H}_2\text{O}^b$	15	35.0
6	$\text{Cu}(\text{OAc})_2 \cdot \text{H}_2\text{O}^c$	10	0.0
7	MCM-41 supported Cu nano	15	45.0

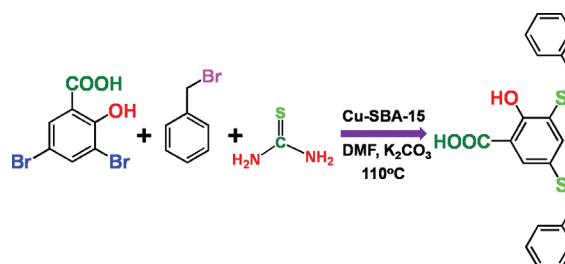
Notes: ^aReaction conditions: bromobenzene (1 mmol, 157 mg), thiophenol (1.1 mmol, 121 mg), K_2CO_3 (2 mmol, 276 mg), DMF (3 ml), reaction temperature: 110°C (oil bath), catalyst: 20 mg; ^bReaction conditions: iodobenzene (1 mmol, 204 mg), thiophenol (1.1 mmol, 121 mg), K_2CO_3 (2 mmol, 276 mg), DMF (3 ml), reaction temperature: 110°C (oil bath), catalyst: $\text{Cu}(\text{OAc})_2 \cdot \text{H}_2\text{O}$, 20 mg; ^cReaction conditions: bromobenzene (1 mmol, 157 mg), thiophenol (1.1 mmol, 121 mg), K_2CO_3 (2 mmol, 276 mg), DMF (3 ml), reaction temperature: 25°C (room temperature), catalyst: $\text{Cu}(\text{OAc})_2 \cdot \text{H}_2\text{O}$ (20 mg).

Table III. Effect of bases for one-pot thioetherification reaction of bromobenzene with benzyl bromide and thiourea over Cu-F-SBA-15 nanocatalyst.^a

Entry	Base	Yield (%) ^b
1	K ₂ CO ₃	82
2	Na ₂ CO ₃	75
3	KOH	60
4	NaOH	60
5	Pyridine	50

Notes: ^aReaction conditions: aryl bromide (1 mmol, bromobenzene, 157 mg), thiourea (1.2 mmol, 91 mg), benzyl bromide (1.1 mmol, 188 mg), base (4 mmol), H₂O (5 ml), reaction temperature: 100 °C (oil bath), Cu-F-SBA-15 nanocatalyst: 25 mg; ^bIsolated yield of the product.

one-pot thioetherification reaction with equal efficiency. –NH₂ substituted chloro compound did not undergo substitution reaction with benzyl bromide in the presence of K₂CO₃ base under the reaction condition. The Cu content of the fresh catalyst was 0.986 mmol g⁻¹, as measured by ICP-AES analysis. A control experiment was conducted by using bromobenzene, benzyl bromide and thiourea but no corresponding product was obtained. In order to clarify the fact that the catalytic activity generated from the Cu sites we have performed the reaction in presence of SBA-15 and furfural-SBA15 under optimized reaction condition but here also no yield of the product was obtained. The homogeneous phase Cu(OAc)₂·H₂O was used as a catalyst for this thioetherification reaction but only 45% product was isolated.⁶⁰ The reaction has been performed in a large-scale by taking 1-bromo-4-nitrobenzene in the 10 mmol scale. Here also desired product benzyl 4-nitrophenyl sulfide was obtained in 86% yield. We have tested the scope of thioetherification reaction by employing different bases considering the reaction of bromobenzene with benzyl bromide and thiourea in aqueous medium (Table III). Various bases such as pyridine, Na₂CO₃ and K₂CO₃ provided the thioethers in moderate to excellent yields (Table III, entries 5, 2 and 1). When NaOH and KOH were used as the base for this thioetherification reaction then both of them provide same yield (Table III, entries 3 and 4). 1, 4-dibromo benzene also undergoes double thioetherification reaction in the presence of benzyl bromide and thiourea under optimized conditions with the corresponding yield 75% (Scheme 5). Similarly 3,5-dibromosalicylic acid undergoes one pot thioetherification reaction to produce bis thioether derivative in DMF solvent (Scheme 6). It produces 72%

**Scheme 5.** One pot thioetherification reaction of 1,4-dibromobenzene using thiourea and benzyl bromide over Cu-F-SBA-15 nanocatalyst (2) in aqueous medium.**Scheme 6.** One pot thioetherification reaction of 3, 5-dibromosalicylic acid using thiourea and benzyl bromide over Cu-F-SBA-15 nanocatalyst (2).

yield in the DMF solvent. Water has not been used here as a solvent as the reaction for this particular compound is very poor in water solvent. We have introduced a comparison data of our Cu-grafted nanocatalysts with the previously reported catalysts in the Table IV. From this Table IV it is clear that our Cu-grafted mesoporous nanocatalysts are more efficient than the other catalysts for performing the C—S coupling and thioetherification reactions.

AAS analysis was carried out to estimate the Cu content for the both nanocatalysts in the fresh form and after the catalysis. After the completion of respective C—S coupling and thioetherification reaction the product was filtered off and washed with acetone and then the filtrate was evaporated to dryness. 30 wt% of nitric acid was added to the filtrate, and the resulting sample adjusted to 5 wt% nitric acid was applied to characterize the Cu leaching. Cu content in the filtrate was analyzed by using a Shimadzu AA-6300 atomic absorption spectrophotometer. Atomic absorption spectrometric analysis of the liquid phase suggested the absence of any detectable amount of Cu in the filtrate solution and that filtrate remains complete colorless. We have verified our results through ICP-AES analysis for both

Table IV. Comparison of Cu-grafted nanocatalysts with the reported previous catalysts.

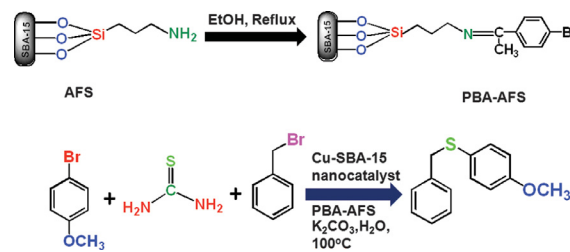
Catalyst	Solvent	Time (h)	Yield (%)	Reference
CuI (2.5 mol %)	NMP	16	92 ^a , 60 ^b	[58]
No reusability				
CuO nanoparticle	DMSO	10	95 ^a , 37 ^c	[61]
Cu/SiO ₂	DMSO	11	83 ^c	[62]
CuI and Phen	Toluene	3	67.2 ^a	[43]
CuO nanopowder	Ionic liquid	2	99 ^d , 27 ^e	[40]
CoCl ₂ ·6H ₂ O/ cationic 2,2'-bipyridyl system	H ₂ O	24 ^a , 48 ^c	85 ^a , 72 ^c	[42]
Cu ₂ O	DMSO	24 ^d	61 ^c	[63]
CuI in	iPrOH	22	90	[64]
Ethylene glycol				
NiO-ZrO ₂	H ₂ O	24	62 ^a	[25]
CuI	Wet PEG 200	24 ^f	80	[59]

Notes: ^aReaction was carried out with iodobenzene; ^bReaction was carried out in aqueous medium; ^cReaction was carried out with bromobenzene; ^dReaction was performed with Cs₂CO₃ base; ^eReaction was performed with K₂CO₃ base; ^fThioetherification reaction was carried out.

the reused nanocatalysts. After 6th reaction cycle the Cu content has been slightly decreased to 0.99 mmol g^{-1} and $0.979 \text{ mmol g}^{-1}$ for the both catalysts Cu-F-MCM-41 nanocatalyst and Cu-F-SBA-15 nanocatalyst, respectively (this decrease is within the experimental error of chemical analysis). This result clearly signifies that Cu sites have been covalently anchored with the organic functional groups inside the backbone of silica unit, which indicates no leaching of Cu occurs from the backbone of mesoporous catalyst during course of reaction under optimized condition.

Hot filtration test was carried out under optimized reaction condition to understand the heterogeneity of our catalytic systems. For the two component C—S coupling reaction 4-bromo anisole (1 mmol, 187 mg), thiophenol (1.1 mmol, 121 mg), K_2CO_3 (2 mmol, 276 mg) and Cu-F-MCM-41 nanocatalyst (25 mg) in 5 ml DMF was heated at 383 K for 4 h. Also for the typical thioetherification reaction 4-bromo anisole (1 mmol, 187 mg), K_2CO_3 (4 mmol, 552 mg), thiourea (1.2 mmol, 91 mg), benzyl bromide (1.1 mmol, 188 mg) and Cu-F-SBA-15 nanocatalyst (25 mg) in 5 ml of H_2O was heated to refluxed at 100°C for 6 h. After a certain time (time included previously i.e., 4 h and 6 h) both the reaction were stopped. The Cu-catalysts were filtered off (from the hot reaction mixture) after 4 h and 6 h, respectively. GC and ^1H NMR data suggests that the 50% conversion was achieved after the scheduled time. Then both reactions were continued with the respective filtrate for another 4 h and 6 h at the same respective reaction temperature. Absolutely no increase in product conversion was achieved beyond 50%. It is further noted that copper is also not detected (AAS) in the liquid phase after the completion of the reactions and the filtrates remain completely colorless.

In order to verify heterogeneous nature of the nanocatalysts a three phase test was performed. In this experiment a desired amount of amino-functionalized silica (AFS) was refluxed with *p*-bromoacetophenone in dry ethanol under nitrogen atmosphere for 5 h. Then the mixture was cooled to room temperature and filtered via repeatedly washing with ethanol to remove unreacted *p*-bromoacetophenone. The material was air dried to obtain the PBA-AFS. Then a mixture of 4-bromo anisole (1 mmol, 187 mg), K_2CO_3 (4 mmol, 552 mg), thiourea (91 mg, 1.2 mmol), benzyl bromide (188 mg, 1.1 mmol) was heated at 100°C for 12 h in presence of Cu-F-SBA-15 nanocatalyst (25 mg) and PBA-PS material. Resulting mixture was then cooled to room temperature, extracted with EtOAc. The combined organic layer was washed with water and brine solution. Then the combined organic layer was dried over anhydrous Na_2SO_4 and evaporated to dryness. The product was analyzed by ^1H NMR, which showed the compound was benzyl 4-methoxyphenyl sulfide. The obtained solid residue was digested refluxing with 2M HCl and the solution was extracted with Et_2O . The obtained



Scheme 7. Three phase test for C—S coupling reaction over Cu-F-MCM-41 nanocatalyst.

benzyl 4-methoxyphenyl sulfide product confirms that 4-bromoacetophenone did not take part in the thioetherification reaction. Absence of any Cu leaching to the solution confirms that anchored *p*-bromoacetophenone did not take part in the thioetherification reaction. Had the copper from Cu-F-SBA-15 nanocatalyst being leached to the solution, the product that could have been obtained would be benzyl 4-formyl sulfide instead of benzyl 4-methoxyphenyl sulfide. Thus, this three-phase test provides further evidence that the reaction is truly heterogeneous in nature and there is no leaching of copper during the course of reaction. The same procedure was followed for the Cu-F-MCM-41 nanocatalyst for the two component C—S coupling reaction. The three phase test reaction scheme was provided in the Scheme 7.

In order to establish recyclability of the nanocatalysts the C—S coupling reaction (4-bromoanisole and thiophenol) and one-pot thioetherification (4-bromo anisole, benzyl bromide and thiourea) were performed under optimized reaction conditions. These two reactions were taken as the representative case. After the reaction was over, the catalyst was separated from the reaction mixture by filtration, washed with copious amount of water followed by diethyl ether. Then the recovered catalysts were dried at room temperature for 6 h and used for further six additional reaction cycles. In all cases Cu-F-MCM-41 and Cu-F-SBA-15 nanocatalysts exhibited consistent catalytic activity, establishing high recycling efficiency of the catalyst and no significant loss of catalytic activity (Fig. 7).

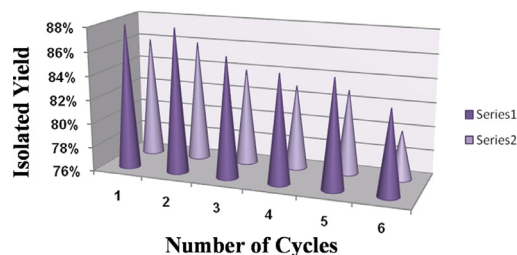


Fig. 7. Recyclable efficiency of the Cu-F-MCM-41 and Cu-F-SBA-15 nanocatalysts. Series 1 = C—S coupling reaction and Series 2 = Thioetherification reaction.

4. CONCLUSIONS

In conclusion we have developed two novel mesoporous furfural-imine functionalized silica anchored Cu nanocatalyst by *in situ* and post grafting methods, respectively. Cu-F-MCM-41 nanocatalyst catalyzed the C—S coupling reaction very efficiently under aerobic condition to offer different bis-thioethers. Also another novel protocol for one-pot thioetherification reaction of different bromo- and chloroarenes with thiourea and benzyl bromide in the presence of K_2CO_3 in aqueous medium was achieved by Cu-F-SBA-15 nanocatalyst under aerobic condition to provide some value added aryl alkyl thioether. This one-pot thioetherification procedure is free from the direct use of volatile, foul-smelling thiols to the address industrial and environmental concerns. Both the nanocatalysts are inexpensive, non-air sensitive, robust and heterogeneous in nature. Both the nanocatalysts can be separated from the reaction mixture easily and recycled for several times without significant loss of catalytic activity. The catalytic activity for these Cu-grafted heterogeneous nanocatalysts for the synthesis of thioethers via two and three component S-arylation reaction could open new avenues in the field of molecular catalysis.

Acknowledgments: John Mondal and Noor Salam thank CSIR, New Delhi and University Grant Commission (UGC) for their respective senior and junior research fellowships. Asim Bhaumik wishes to thank DST Unit on Nanoscience for instrumental support.

References and Notes

- C. Burda, Z. Chen, R. Narayanan, and M. A. El-Sayed, *Chem. Rev.* 105, 1025 (2005).
- S. Laurent, D. Forge, M. Port, A. Roch, C. Robic, L. V. Elst, and R. N. Muller, *Chem. Rev.* 108, 2064 (2008).
- X. T. Chen, A. Yamaguchi, M. Namekawa, T. Kamijo, N. Teramae, and A. J. Tong, *Anal. Chim. Acta* 696, 94 (2011).
- S. Panigrahi, S. Basu, S. Praharaj, S. Pande, S. Jana, A. Pal, S. K. Ghosh, and T. Pal, *J. Phys. Chem. C* 111, 4596 (2007).
- S. Ogasawara and S. Kato, *J. Am. Chem. Soc.* 132, 4608 (2010).
- V. Polshettiwar, B. Baruwati, and R. S. Varma, *ACS Nano* 3, 728 (2009).
- S. Jammi, S. Sakthivel, L. Rout, T. Mukherjee, S. Mandai, R. Mitra, P. Saha, and T. Punniyamurthy, *J. Org. Chem.* 74, 1971 (2009).
- B. J. Borah, D. Dutta, P. P. Saikia, N. C. Barua, and D. K. Dutta, *Green Chem.* 13, 3453 (2011).
- W. Boettcher, J. M. Spurgeon, M. C. Putnam, E. L. Warren, D. B. Turner-Evans, M. D. Kelzenberg, J. R. Maiolo, H. A. Atwater, and N. S. Lewis, *Science* 327, 185 (2010).
- F. Alonso, Y. Moglie, G. Radivoy, and M. Yusa, *Adv. Synth. Catal.* 352, 3208 (2010).
- J. L. Li, D. S. Zhen, G. Z. Sui, C. M. Zhang, Q. G. Deng, and L. H. Jia, *J. Nanosci. Nanotechnol.* 12, 6265 (2012).
- A. K. Patra, A. Dutta, and A. Bhaumik, *Catal. Commun.* 11, 651 (2010).
- M. Kidwai, N. K. Mishra, S. Bhardwaj, A. Jahan, A. Kumar, and S. Mozzumdar, *ChemCatChem* 2, 1312 (2010).
- R. A. Sheldon, *Green Chem.* 9, 1273 (2007).
- M. Kidwai, S. Bhardwaj, N. K. Mishra, A. Jain, A. Kumar, and S. Mozzumdar, *Catal. Sci. Technol.* 1, 426 (2011).
- M. Kaya, M. Zahmakiran, S. Ozkar, and M. Volkan, *ACS Appl. Mater. Interfaces* 4, 3866 (2012).
- J. Y. Kim, J. C. Park, H. Kang, H. Song, and K. H. Park, *Chem. Commun.* 46, 439 (2010).
- H. Sharghi, R. Khalifeh, and M. M. Doroodmanda, *Adv. Synth. Catal.* 351, 207 (2009).
- G. Molteni, C. L. Bianchi, G. Marinoni, N. Santod, and A. Ponti, *New J. Chem.* 30, 1137 (2006).
- B. H. Lipshutz, D. M. Nihan, E. Vinogradova, B. R. Taft, and Z. V. Boskovic, *Org. Lett.* 10, 4279 (2008).
- I. S. Park, M. S. Kwon, Y. Kim, J. S. Lee, and J. Park, *Org. Lett.* 10, 497 (2008).
- A. Nakajima, Y. Akiyama, S. Yanagida, T. Koike, T. Isobe, Y. Kameshima, and K. Okada, *Mater. Lett.* 63, 1699 (2009).
- T. Tsoncheva, V. D. Santo, A. Gallo, N. Scotti, M. Dimitrov, and D. Kovacheva, *Appl. Catal. A: Gen.* 406, 13 (2011).
- J. Mondal, T. Sen, and A. Bhaumik, *Dalton Trans.* 41, 6173 (2012).
- N. Pal and A. Bhaumik, *Dalton Trans.* 41, 9161 (2012).
- Y. Kubota, H. Yamaguchi, T. Yamada, S. Inagaki, Y. Sugi, and T. Tatsumi, *Top. Catal.* 492, 53 (2010).
- D. Chandra, S. K. Das, and A. Bhaumik, *Microporous Mesoporous Mater.* 128, 34 (2010).
- N. Mizoshita, T. Tani, and S. Inagaki, *Chem. Soc. Rev.* 789, 40 (2011).
- M. Hartmann, S. Racouchot, and C. Bischof, *Microporous Mesoporous Mater.* 27, 309 (1999).
- L. Chmielarz, P. Kustrowski, R. Dziembaj, P. Cool, and E. F. Vansant, *Appl. Catal. B: Environ.* 62, 369 (2006).
- C.-C. Chan, Y.-W. Chen, C.-S. Su, H.-P. Lin, and C.-F. Lee, *Eur. J. Org. Chem.* 7288 (2011).
- Z. Wu, Y. Wang, W. Huang, J. Yang, H. Wang, J. Xu, Y. Wei, and J. Zhu, *Chem. Mater.* 19, 1613 (2007).
- Q. H. Zhang, W. P. Deng, and Y. Wang, *Chem. Commun.* 47, 9275 (2011).
- M. Nandi, P. Roy, H. Uyama, and A. Bhaumik, *Dalton Trans.* 40, 12510 (2011).
- L. Liu, J. E. Stelmach, S. R. Natarajan, M.-H. Chen, S. B. Singh, C. D. Schwartz, C. E. Fitzgerald, S. J. O'Keefe, D. M. Zaller, D. M. Schmatz, and J. B. Doherty, *Bioorg. Med. Chem. Lett.* 13, 3979 (2003).
- J. P. Wolfe, S. Wagaw, J. F. Marcoux, and S. L. Buchwald, *Acc. Chem. Res.* 31, 805 (1998).
- T. Kondo and T. A. Mitsudo, *Chem. Rev.* 100, 3205 (2000).
- G. Liu, J. R. Huth, E. T. Olejniczak, F. Mendoza, S. W. Fesik, and T. W. von Geldern, *J. Med. Chem.* 44, 1202 (2001).
- G. De Martino, M. C. Edler, G. La Regina, A. Cosuccia, M. C. Barbera, D. Barrow, R. I. Nicholson, G. Chiosis, A. Brancale, E. Hamel, M. Artico, and R. Silvestri, *J. Med. Chem.* 49, 947 (2006).
- R. S. Schwab, D. Singh, E. E. Alberto, P. Piquini, O. E. D. Rodrigues, and A. L. Braga, *Catal. Sci. Technol.* 1, 569 (2011).
- J. Mondal, A. Modak, A. Dutta, and A. Bhaumik, *Dalton Trans.* 40, 5228 (2011).
- M.-T. Lan, W.-Y. Wu, S.-H. Huang, K.-L. Luo and F.-Y. Tsai, *RSC Adv.* 1, 1751 (2011).
- S.-W. Cheng, M.-C. Tseng, K.-H. Lii, C.-R. Lee, and S.-G. Shyu, *Chem. Commun.* 47, 5599 (2011).
- A. M. Fernández-Rodríguez, and J. F. Hartwig, *Chem.–Eur. J.* 16, 2355 (2010).
- Z. Jiang, J. She, and X. Lin, *Adv. Synth. Catal.* 351, 2558 (2009).
- J. Zhang, C. M. Medley, J. A. Krause, and H. Guan, *Organometallics* 29, 6393 (2010).
- V. K. Akkilagunta, V. P. Reddy, and K. R. Rao, *Synlett.* 8, 1260 (2010).
- V. P. Reddy, A. V. Kumar, K. Swapna, and K. R. Rao, *Org. Lett.* 11, 1697 (2009).

49. H. Firouzabadi, N. Iranpoor, and M. Abbasi, *Tetrahedron* 65, 5293 (2009).
50. J. Mondal, A. Modak, A. Dutta, S. Basu, S. N. Jha, D. Bhattacharyya, and A. Bhaumik, *Chem. Commun.* 48, 8000 (2012).
51. K. Sarkar, M. Nandi, M. Islam, T. Mubarak, and A. Bhaumik, *Appl. Catal. A: Gen.* 352, 81 (2009).
52. V. S. G.-Cuello, L. Giraldo, and J. C. M.-Pirajan, *J. Chem. Eng. Data* 56, 1167 (2011).
53. M. S. E.-Shall, V. Abdelsayed, A. E. R. S. Khder, H. M. A. Hassan, H. M. E.-Kaderi, and T. E. Reich, *J. Mater. Chem.* 19, 7625 (2009).
54. Y.-C. Fang, H.-C. Lin, I.-J. Hsu, T.-S. Lin, and C.-Y. Mou, *J. Phys. Chem. C* 115, 20639 (2011).
55. Y. Li, Y. Hu, S. Peng, G. Lu, and S. Li, *J. Phys. Chem. C* 113, 9352 (2009).
56. J. Wang, W. J. Wang, B. Song, R. Wu, J. Li, Y. F. Sun, Y. F. Zheng, and J. K. Jian, *J. Nanosci. Nanotechnol.* 10, 3131 (2010).
57. ^1H and ^{13}C NMR chemical shifts for different coupling products reported in Table I
- Di phenyl sulfide (Table I, entry 1):** ^1H NMR (300 MHz, CDCl_3) δ = 7.519–7.109 (5H, m); ^{13}C NMR (300 MHz, CDCl_3) δ = 137.6, 131.1, 129.2, 124.9.
- 4-Phenylsulfanylanisole (Table II, entry 2):** ^1H NMR (300 MHz, CDCl_3) δ 3.78 (s, 3H), 6.98 (d, J = 8.7 Hz, 2H), 7.17–7.21 (m, 5H), 7.40 (d, J = 9.0 Hz, 2H); ^{13}C NMR (75 MHz, CDCl_3) δ 55.2, 115.0, 124.2, 125.7, 128.2, 128.9, 135.3, 138.6, 159.8.
- 4-Phenylsulfanylbenzaldehyde (Table I, entry 3):** ^1H NMR (500 MHz, CDCl_3) δ 9.82 (s, 1H), 7.658–7.641 (d, J = 8.5 Hz, 2H), 7.590–7.577 (d, J = 6.5 Hz, 2H), 7.446–7.426 (d, J = 10 Hz, 2H), 7.22–7.15 (m, 3H); ^{13}C NMR (500 MHz, CDCl_3) δ 190.7, 146.9, 136.8, 134.1, 132.2, 131.2, 130.8, 129.6, 127.3.
- 4-Phenylsulfanylbenzotrile (Table I, entry 4):** ^1H NMR (500 MHz, CDCl_3) δ 7.31–7.38 (m, 4H), 7.20 (d, 2H), 7.06–6.96 (m, 3H); ^{13}C NMR (500 MHz, CDCl_3) δ 142.1, 135.7, 132.8, 131.9, 131.2, 129.4, 127.3, 117.8, 111.2.
- 4-Phenylsulfanylbenzoicacid (Table I, entry 5):** ^1H NMR (500 MHz, CDCl_3) δ 7.52–7.51 (d, J = 8 Hz, 4H), 7.312–7.302 (t, J = 7 Hz, 4H), 7.240–7.225 (t, J = 7.5 Hz, 1H); ^{13}C NMR (500 MHz, CDCl_3) δ 171.0, 137.0, 129.0, 127.5, 127.1.
- 4-Phenylsulfanylacetophenone (Table I, entry 6):** ^1H NMR (500 MHz, CDCl_3) δ 7.665–7.648 (d, J = 8.5 Hz, 2H), 7.350–7.335 (d, J = 7.5 Hz, 2H), 7.241–7.228 (d, J = 6.5 Hz, 2H), 7.061–7.006 (m, 3H); ^{13}C NMR (500 MHz, CDCl_3) δ 196.9, 145.9, 135.7, 134.0, 131.9, 131.3, 129.6, 129.5, 126.8, 29.6.
- 3-Phenylsulfanylbenzaldehyde (Table I, entry 7):** ^1H NMR (500 MHz, CDCl_3) δ 9.92 (s, 1H), 7.98 (s, 1H), 7.786–7.771 (d, J = 7.5 Hz, 2H), 7.49–7.371 (m, 3H), 7.322–7.186 (m, 3H); ^{13}C NMR (500 MHz, CDCl_3) δ 191.5, 138.0, 137.2, 136.9, 135.2, 132.2, 131.0, 129.1, 128.3, 127.6, 127.1.
- 4-Phenylsulfanyl nitrobenzene (Table I, entry 8):** ^1H NMR (500 MHz, CDCl_3) δ 7.987–7.970 (d, J = 8.5 Hz, 2H), 7.495–7.476 (d, J = 7.5 Hz, 2H), 7.440–7.394 (m, 3H), 7.120–7.102 (d, J = 9 Hz, 2H); ^{13}C NMR (500 MHz, CDCl_3) δ 148.2, 145.2, 136.8, 132.4, 130.3, 128.9, 127.3, 123.8.
- 4-methyl-2-phenylsulfanylaniline (Table I, entry 9):** ^1H NMR (500 MHz, CDCl_3) δ 7.522–7.507 (d, J = 7.5 Hz, 2H), 7.454–7.7.175 (m, 4H), 6.914–6.896 (d, J = 9 Hz, 1H), 6.650–6.636 (d, J = 7 Hz), 3.914 (s, 2H), 2.234 (s, 3H); ^{13}C NMR (500 MHz, CDCl_3) δ 141.4, 136.8, 132.4, 130.9, 129.1, 128.9, 127.4, 126.9, 115.8, 20.9.
- 2-Phenylsulfanylbenzaldehyde (Table I, entry 10):** ^1H NMR (500 MHz, CDCl_3) δ 10.2 (s, 1H), 7.846–7.828 (d, J = 9 Hz, 1H), 7.442–7.426 (d, J = 8 Hz, 1H), 7.377–7.311 (m, 6H), 7.161–7.035 (m, 1H); ^{13}C NMR (500 MHz, CDCl_3) δ 191.1, 141.3, 136.8, 135.1, 133.9, 132.9, 131.6, 129.6, 128.9, 128.3, 127.3.
- Di benzyl phenyl disulfide (Scheme 5):** ^1H NMR (300 MHz, CDCl_3) δ 7.11–7.28 (m, 14H), 3.49 (4H, s); ^{13}C NMR (300 MHz, CDCl_3) δ 137.7, 132.6, 128.9, 127.9, 126.8, 126.3, 42.6.
- Di benzyl 2-hydroxy-1-carboxy phenyl disulfide (Scheme 6):** ^1H NMR (300 MHz, CDCl_3) δ 7.62–7.54 (t, 1H), 7.49–7.7.42 (m, 1H), 7.37–7.13 (m, 10H), 3.89 (s, 4H); ^{13}C NMR (300 MHz, CDCl_3) δ 171.0, 153.4, 137.2, 129.6, 129.2, 128.6, 128.1, 127.6, 127.4, 125.6, 43.1.
58. E. Sperotto, G. P. M. van Klink, J. G. de Vries, and G. van Koten, *J. Org. Chem.* 73, 5625 (2008).
59. H. Firouzabadi, N. Iranpoor, and M. Gholinejada, *Adv. Synth. Catal.* 352, 119 (2010).
60. V. Polshettiwar, J.-M. Basset, and D. Astruc, *ChemSusChem* 5, 6 (2012).
61. L. Rout, T. K. Sen, and T. Punniyamurthy, *Angew. Chem.* 119, 5679 (2007).
62. P. Veerakumar, M. Velayudham, K.-L. Lub, and S. Rajagopal, *Catal. Sci. Technol.* 1, 1512 (2011).
63. H.-J. Xu, X.-Y. Zhao, J. Deng, Y. Fu, and Y.-S. Feng, *Tetrahedron Lett.* 50, 434 (2009).
64. F. Y. Kwong and S. L. Buchwald, *Org. Lett.* 4, 3517 (2002).

Received: 17 October 2012. Accepted: 14 February 2013.